ChemPubSoc Europe

DOI: 10.1002/chem.202000158

CHEMISTRY A European Journal Communication

Ligand Effects

Dual Metastability in Electroless Plating: Complex Inertness Enabling the Deposition of Composition-Tunable Platinum Copper Alloy Nanostructures

Tobias Stohr,[a] Joachim Brötz,[a] Mehtap Oezaslan,[b, c] and Falk Muench*[a]

Abstract: Autocatalytic deposition represents a facile, versatile, and scalable wet-chemical tool for nanofabrication. However, the intricate component interplay in plating baths containing multiple metal species impedes alloy deposition. We resolved this challenge in the bimetallic copper-platinum system by exploiting the kinetic stability of platinum complexes, which allows adjusting their ligand sphere and thus reactivity independently from the present copper ions in a preceding, thermally activated ligand exchange step. By using metastable Pt^{IV} precursors of varying degrees of complexation, copper-platinum alloys of adjustable atomic ratio were plated from solutions of identical composition and concentration, but differing local coordination environment. Due to its excellent conformity and nanoscale homogeneity, the reaction is compatible with ambitious 3D substrate morphologies, as demonstrated in the template-assisted fabrication of nanotubes with high aspect ratio. The ability to generate additional synthetic degrees of freedom by decoupling the metal complex speciation from the solution composition is of large interest for redox-chemical synthesis techniques, such as electrodeposition or nanoparticle colloid production.

Autocatalytic deposition, also referred to as chemical or electroless plating, is an industrially well-established, wet-chemical reaction class used for the conformal metallization of almost arbitrary work pieces.[1] Mechanistically, this process is related to electrodeposition, with the notable distinction that the electrons needed for metal-ion reduction are not externally supplied, but generated in situ by the oxidation of reducing agents. While the plating baths tend to decompose into elemental metals and oxidized reducing agents, this conversion is kinetically suppressed to a large extent. The activation barrier can be overcome by heterogeneous catalytic action, enabling selective deposition on catalytic surfaces and the continued growth of the plated, autocatalytic metal films.

Due to its efficiency, autocatalytic deposition is a compelling tool for nanofabrication. High quality nanoscale metal coatings can be obtained by simply submerging substrates in aqueous plating baths at ambient temperatures.[2–8] The outstanding conformity of the reaction allows replicating the shape of intricate templating scaffolds,[2–5,7] providing access to sophisticated nano-architectures such as arrays,[2,5] networks[4,5] or multiscale hierarchical lattices[3] composed of metal nanotubes. Stopping plating at early stages allows producing island-like metal nanoparticle films,[6] and shape-controlled reaction variants can be used to directly coat surfaces with nanowires,[8] nanoplates,[8] or nanospikes.[4]

Despite their technological importance,[9] alloy nanomaterials are not often produced by autocatalytic deposition, apart from two notable exceptions: (i) combinations of the chemically similar iron group metals Fe, Co and Ni[10] and (ii) alloys containing heteroatoms like P or B formed as byproducts from from the employed reducing agents.[10] The relative scarcity of autocatalytic alloy plating reactions in general and comprising noble metals in particular is related to their strong focus on nickel- or copper-based protective and conductive coatings,[1,10] as well as to their complexity.

Compared to electroplating, alloy deposition is considerably more intricate in autocatalytic systems. Here, the electrode potential as the pivotal driving force cannot be freely and dynamically controlled, but is determined in situ by the interplay of the oxidation and reduction half reactions simultaneously proceeding on the deposit.[1] All included metals must be deposited at comparable rates under these confined conditions, and techniques such as pulsed deposition cannot be used to cross reducibility gaps or to tune the alloy composition.[11] The autocatalytic qualities of the metallic deposit governing the plating reaction are a strong function of its composition, and thus

[a] T. Stohr, Dr. J. Brötz, Dr. F. Muench
Department of Materials and Earth Sciences
Technische Universität Darmstadt
64287 Darmstadt (Germany)
E-mail: muench@ma.tu-darmstadt.de

[b] Prof. Dr. M. Oezaslan
Institute of Technical Chemistry
Technische Universität Braunschweig
Hagenring 30, 38106 Braunschweig (Germany)

[c] Prof. Dr. M. Oezaslan
Department of Chemistry
Carl von Ossietzky University of Oldenburg
26111 Oldenburg (Germany)

Supporting information and the ORCID identification number(s) for the author(s) of this article can be found under: https://doi.org/10.1002/chem.202000158.

markedly altered in alloys.[12] Chemical metastability is challenging to achieve, more so simultaneously for multiple species: Adding ions of a more reactive metal to an autocatalytic deposition solution brings the risk of uncontrolled reduction, resulting in homogeneous nucleation and bath decomposition.[12] While this reactivity can be exploited for seeding bimetallic nanoparticle colloids by homogeneous nucleation of noble metal cores,[13] it is inappropriate for surface-selective and alloy depositions. Aside the reducer, additives[14] and ligands can also cause interferences. For instance, while complexation represents a powerful strategy for tailoring the electrochemical reactivity,[15,16] limitations arise due to the concurrent effect of ligands on all present metal ions.

Herein, we highlight how this interference can be overcome by exploiting a curious feature of platinum complexes: Their kinetic stability[17] allows predefining the coordination environment of the platinum precursor, effectively decoupling its composition from the ligands present in the plating solution. This strategy provides independent control over the platinum complex reactivity, which remains locked after addition to the plating bath. Using ligand-shell engineering to systematically vary the degree of platinum precursor stabilization, we are able to autocatalytically deposit composition-tunable copper–platinum alloy nanofilms from solutions of identical global composition. Intriguingly, those solutions exhibit dual metastability, with respect to both metal reduction and ligand exchange at the platinum center.

Due to its previous successful implementation in autocatalytic deposition,[18] we chose ethylenediamine (en) for Pt^{IV} complexation. Starting from $[PtCl_6]^{2-}$, up to three en units can be attached, each replacing two chloride ions upon chelation (Figure 1 A). UV/Vis spectroscopy was used to confirm the inertness of the Pt^{IV} species in our reaction system. To this end, four different degrees of complexation were realized by mixing $[PtCl_6]^{2-}$ solutions with 0, 1.3, 2.7, and 4 equivalents of en, spanning the complete range from unaltered to fully ligand-exchanged Pt^{IV} species using a slight en excess. During heating, the color of the initially orange–yellow solutions faded to (pale) yellow, with the extent of color change depending on the amount of added en, indicating different levels of ligand exchange. In the following, we use the number *n* of en equivalents applied in the temperature-facilitated ligand exchange step (Figure 1 B) to denote our experiments. After cooling down to room temperature, each solution was balanced with en to reach a total of four ligand equivalents (Figure 1 B), and mixed with diluted NaOH to mimic the alkalinity of the plating baths the Pt^{IV} species are added to later (Supporting Information, Section S1.5).

The distinct variance of the UV/Vis spectra strikingly contrasts the globally identical composition of the solutions and immediately corroborates the differing nature of the present Pt^{IV} complexes (Figure 1 C,D). Notably, it is found after en balancing, providing clear evidence for the Pt^{IV} complex inertness in our system: The history of solution preparation counts, not the overall amount of added ligand. Absorption bands are found around 450, 370, and 260 nm, which have been previously assigned to (partially spin-forbidden) d–d transitions

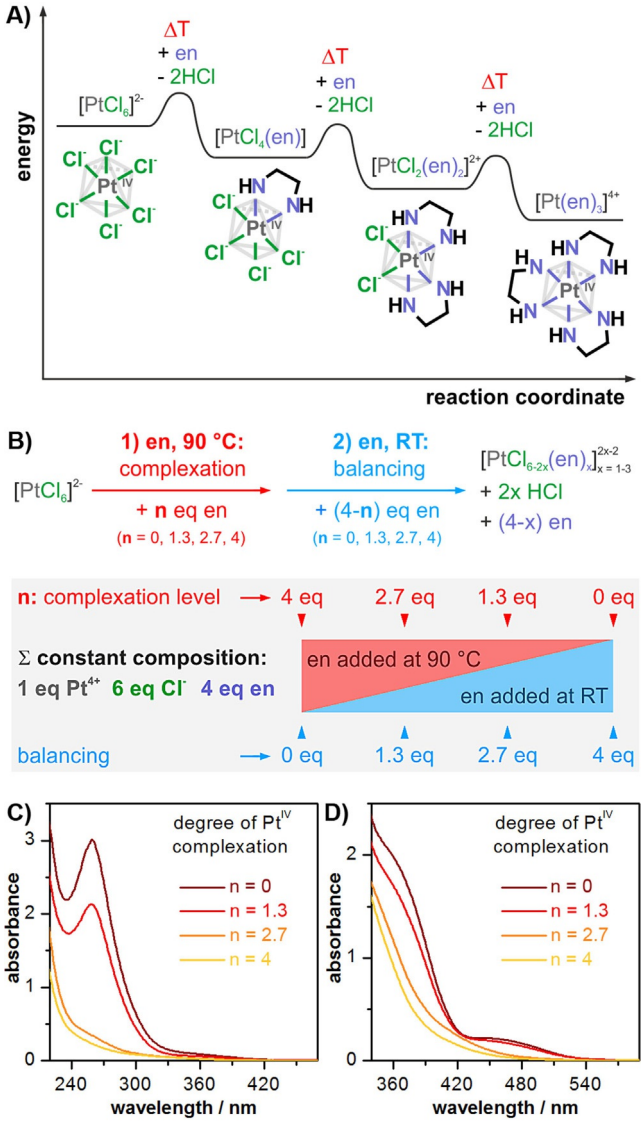

Figure 1. A) Scheme showing the different levels of ligand exchange at $[PtCl_6]^{2-}$, which acts as Pt^{IV} precursor in our synthesis. B) Preparation Scheme of the solutions for spectrophotometric analysis. UV/Vis spectra of the complex solutions: C) diluted 30-fold with water, D) as-prepared (n denotes the equivalents of en used for Pt(IV) complexation).

($^1A_{1g} \rightarrow {}^1T_g/{}^3T_g$) and ligand-to-metal charge-transfer bands ($t_{2u} \rightarrow e_g$) in $[PtCl_6]^{2-}$.[19,20] With an increasing fraction of en added at elevated temperature, all absorption bands decrease in intensity, pointing out the increasing substitution of chloride by en. While aquation also must be considered[19] and chloride can be completely replaced by hydroxide—although this process is thermally activated as well[20]—efficient solvolysis can be ruled out in our case: The peak centered around 260 nm, which is characteristic for the chloride-to-metal charge transfer band and disappears in the hydroxo complex,[20] is pronounced in the samples of low en complexation ($n = 0$, 1.3). Its absence in the most substituted sample ($n = 4$) verifies total chloride ion replacement by en.

Cu–Pt alloy deposition was achieved by adding four different Pt^{IV} solutions ($n = 0$, 1.3, 2.7, 4) prepared alike to those utilized in the spectroscopic studies to alkaline, formaldehyde-

based[21] electroless copper plating baths (Supporting Information, Section S1.4). The final plating baths featured a constant en content of 245 mM. Ion-track etched polycarbonate membranes were used as model substrates for the template-assisted synthesis of 1D nanostructures.[2,4] These membranes incorporate channel-shaped pores of high aspect ratio, and therefore represent an excellent platform for testing the nanoscale homogeneity and conformity of the deposit. Being intrinsically inactive, polymer membranes have to be decorated with catalytic metal nanoparticles like Ag or Pd prior to plating in order to initiate metallization.[2,4] Opposed to the autocatalytic deposition of pure copper [Eq. 1], the Cu–Pt depositions have not been accompanied by strong gas evolution. This hints at the catalytic interference of elemental platinum, onto which formaldehyde is oxidized together with detached H atoms, preventing H_2 recombination [Eq. 2]:[12,21]

$$HCHO + 2\,OH^- \rightarrow HCOO^- + {}^1/_2\,H_2 \uparrow + H_2O + e^- \quad (1)$$

$$HCHO + 3\,OH^- \rightarrow HCOO^- + 2\,H_2O + 2\,e^- \quad (2)$$

The optical appearance of the metallized foils ranged from anthracite for the pristine $[PtCl_6]^{2-}$ to coppery for the most substituted Pt^{IV} complex, suggesting that increased platinum stabilization translates to reduced incorporation into the deposit (Figure 2). Energy-dispersive *x*-ray spectroscopy (EDS) confirms this anticipated behavior, finding at% compositions of $Cu_{79}Pt_{21}$ ($n=0$), $Cu_{87}Pt_{13}$ ($n=1.3$), $Cu_{95}Pt_5$ ($n=2.7$), and $Cu_{98}Pt_2$ ($n=4$).

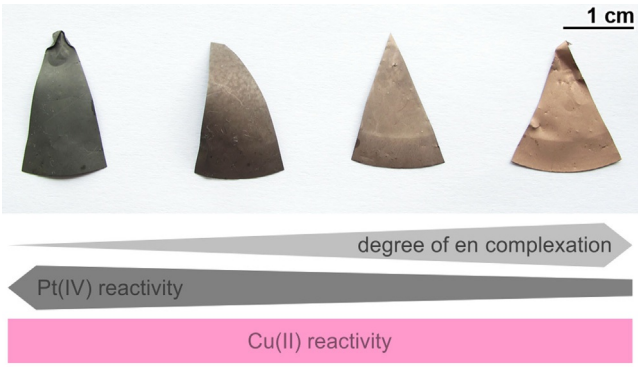

Figure 2. Photographs of metallized polycarbonate templates obtained with different complexation levels ranging from pristine $[PtCl_6]^{2-}$ (left) to fully chelated Pt^{IV} (right).

SEM revealed the successful formation of bimetallic nanotubes, which endured the template dissolution without noticeable fragmentation and spanned the entire template thickness of ≈30 μm (Figure 3A). As a result of efficient nucleation with high areal density,[22] the tubes tightly replicate the cylindrical shape of the template pores and possess compact walls of relatively even thickness (Figure 3B). Investigating the material with TEM exposed the nanoparticulate quality of the deposit, which is composed of fine grains of <5 nm particle size (Figure 3C,D).

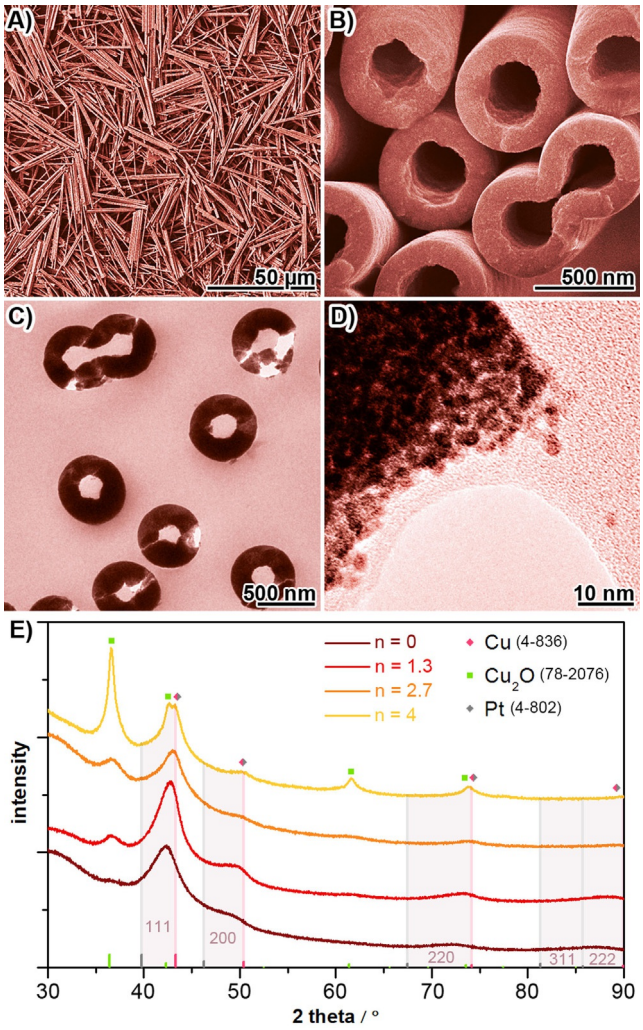

Figure 3. SEM images of template-freed Cu-Pt nanotubes ($n=0$), showing A) a drop-coated film and B) a bundle of tube openings. TEM images of a microtome-cut, metallized template ($n=0$), displaying C) nanotube cross-sections and D) the nanoparticulate structure of the deposit. E) XRD patterns of template-embedded Cu-Pt nanotubes, complemented with ICDD powder standards. The shaded areas highlight the *fcc* reflex positions confined by the parent metals.

In agreement with the small particle size, XRD yielded considerably broadened reflexes. Aside from a pronounced background related to the amorphous polycarbonate substrate, all samples exhibit reflexes corresponding to a face-centered cubic (*fcc*) phase (Figure 3E). The corresponding lattice constants lie in between those of the parent metals, implying that the deposit consists of a disordered Pt–Cu alloy rather than a heterostructure of unalloyed individual metals. The lattice constants monotonically increase with increasing Cu content, approaching the values of pure copper in the case of the most Cu-rich sample ($n=4$), in agreement with the EDS results showing the presence of only few at% of Cu. In the case of the most Pt-rich sample, the reflexes are closely located to the positions expected for $PtCu_3$ (Supporting Information, Figure S2), again matching the composition estimate by EDS ($Pt_{21}Cu_{79}$). All samples show signs of oxidation (presence of cuprous oxide), the extent of which decreases with the nobility

of the alloys. The most Pt-rich sample ($n=0$) only contains a minor contribution of Cu_2O phase (see the hump at the position of the most intense Cu_2O powder reflex, $\approx 36^\circ$). On the contrary, the same Cu_2O reflex is dominating the diffractogram of most Cu-rich sample ($n=4$). In summary, the XRD analysis confirms the successful deposition of Cu–Pt solid solutions of tunable composition. Particularly the Cu-rich alloys are prone to attack by atmospheric oxygen. XPS with optional sputtering shows that the oxidation is limited to the deposit surface (Supporting Information, Figures S3–S5), proving the full reduction of both metal precursors during plating.

In this communication, we outlined a reaction system for the highly conformal and autocatalytic deposition of nanocrystalline Cu–Pt alloy films, the composition of which can be controlled by tuning the Pt^{IV} precursor reactivity in an initial, temperature-assisted ligand exchange step. Plating was performed at low temperatures, at which the predefined Pt^{IV} reactivity is preserved in spite of the presence of an almost 50-fold excess of the thermodynamically preferred en ligand (245 mM en versus 5 mM H_2PtCl_6). Our approach harnesses the kinetic stability of Pt^{IV} complexes to generate an additional degree of synthetic freedom, allowing us to adjust the ligand environment of the platinum precursor independently from the overall solution composition. It represents a fully wet-chemical, facile, scalable, and flexible route for fabricating nanostructures of controlled Cu–Pt ratios, which can be employed as electrocatalysts in, for example, alcohol oxidation[23] or oxygen reduction.[24] Dealloying[23,25] the as-deposited Cu–Pt nanostructures can be used to further tune the material composition and morphology (Supporting Information, Figure S1).

Our strategy represents a starting point for devising new autocatalytic alloy plating reactions involving other metastable metal centers (e.g., Ru^{II}, Os^{II}, Ir^{III})[17] and metal combinations. Also, it is interesting for mechanistically related reactions such as electrodeposition,[15] galvanic displacement,[5] or colloidal nanoparticle synthesis,[16] which benefit alike from the ability to independently adjust the reducibility of individual ions in systems the global composition of which is dictated by external requirements.

Acknowledgements

T.S. is grateful for the support of the German Federal Ministry of Education and Research (BMBF, contract number 05 K16 RDC, project HI-EXE). In addition, we thank the Prof. Biesalski (Technische Universität Darmstadt) for providing access to the spectrophotometer, Prof. C. Trautmann (GSI Helmholtzzentrum für Schwerionenforschung, Darmstadt) for support with the template preparation and for access to the scanning electron microscope, the Zentraleinrichtung Elektronenmikroskopie and Prof. Dr. P. Strasser (Technische Universität Berlin) for their assistance, and C. Kipper for synthetic support.

Conflict of interest

The authors declare no conflict of interest.

Keywords: autocatalytic deposition · copper-platinum alloys · kinetic complex stability · ligand effects · template synthesis

[1] a) H. Niederprüm, *Angew. Chem. Int. Ed. Engl.* **1975**, *14*, 614–620; *Angew. Chem.* **1975**, *87*, 652–658; b) *Electroless Plating: Fundamentals and Applications* (Eds.: G. O. Mallory, J. B. Hajdu), American Electroplaters and Surface Finishers Society, Orlando, FL, **1990**.
[2] S. Papp, G. Jágerszki, R. E. Gyurcsányi, *Angew. Chem. Int. Ed.* **2018**, *57*, 4752–4755; *Angew. Chem.* **2018**, *130*, 4842–4845.
[3] X. Zheng, W. Smith, J. Jackson, B. Moran, H. Cui, D. Chen, J. Ye, N. Fang, N. Rodriguez, T. Weisgraber, C. M. Spadaccini, *Nat. Mater.* **2016**, *15*, 1100–1107.
[4] T. Boettcher, S. Schaefer, M. Antoni, T. Stohr, U. Kunz, M. Duerrschnabel, L. Molina-Luna, W. Ensinger, F. Muench, *Langmuir* **2019**, *35*, 4246–4253.
[5] F. Muench, *Catalysts* **2018**, *8*, 597.
[6] a) F. Muench, A. Solomonov, T. Bendikov, L. Molina-Luna, I. Rubinstein, A. Vaskevich, *ACS Appl. Biol. Mater.* **2019**, *2*, 856–864; b) M. D. Susman, Y. Feldman, A. Vaskevich, I. Rubinstein, *Chem. Mater.* **2012**, *24*, 2501–2508.
[7] N. M. K. Kuruppu Arachchige, P. C. Chambers, A. M. Taylor, Z. L. Highland, J. C. Garno, *ACS Appl. Nano Mater.* **2019**, *2*, 2193–2203.
[8] a) F. Muench, R. Popovitz-Biro, T. Bendikov, Y. Feldman, B. Hecker, H. Oezaslan, I. Rubinstein, A. Vaskevich, *Adv. Mater.* **2018**, *30*, 1805179; b) F. Muench, S. Schaefer, L. Hagelüken, L. Molina-Luna, M. Duerrschnabel, H.-J. Kleebe, J. Brötz, A. Vaskevich, I. Rubinstein, W. Ensinger, *ACS Appl. Mater. Interfaces* **2017**, *9*, 31142–31152.
[9] J.-M. Yan, S.-J. Li, S.-S. Yi, B.-R. Wulan, W.-T. Zheng, Q. Jiang, *Adv. Mater.* **2018**, *30*, 1703038.
[10] J. Sudagar, J. Lian, W. Sha, *J. Alloys Compd.* **2013**, *571*, 183–204.
[11] B. Yoo, F. Xiao, K. N. Bozhilov, J. Herman, M. A. Ryan, N. V. Myung, *Adv. Mater.* **2007**, *19*, 296–299.
[12] J. E. A. M. van den Meerakker, J. W. G. de Bakker, *J. Appl. Electrochem.* **1990**, *20*, 85–90.
[13] L. Lu, I. Sevonkaev, A. Kumar, D. V. Goia, *Powder Technol.* **2014**, *261*, 87–97.
[14] J. Bielinski, K. Kaminski, *Surf. Coat. Technol.* **1987**, *31*, 223–233.
[15] D. Liang, G. Zangari, *Langmuir* **2014**, *30*, 2566–2570.
[16] N. Ortiz, R. G. Weiner, S. E. Skrabalak, *ACS Nano* **2014**, *8*, 12461–12467.
[17] J. Reedijk, *Platinum Met. Rev.* **2008**, *52*, 2–11.
[18] F. Muench, S. Kaserer, U. Kunz, I. Svoboda, J. Brötz, S. Lauterbach, H.-J. Kleebe, C. Roth, W. Ensinger, *J. Mater. Chem.* **2011**, *21*, 6286–6291.
[19] E. L. Cox, D. G. Peters, E. L. Wehry, *J. Inorg. Nucl. Chem.* **1972**, *34*, 297–305.
[20] S. Alerasool, D. Boecker, B. Rejai, R. D. Gonzalez, *Langmuir* **1988**, *4*, 1083–1090.
[21] M. Zhao, L. Yu, R. Akolkar, A. B. Anderson, *J. Phys. Chem. C* **2016**, *120*, 24789–24793.
[22] Y. Wang, S. Luo, K. Ren, S. Zhao, Z. Chen, W. Li, J. Guan, *J. Mater. Chem. C* **2016**, *4*, 2566–2578.
[23] X. Zhang, W. Lu, J. Da, H. Wang, D. Zhao, P. A. Webley, *Chem. Commun.* **2009**, 195–197.
[24] P. Strasser, S. Koh, T. Anniyev, J. Greeley, K. More, C. Yu, Z. Liu, S. Kaya, D. Nordlund, H. Ogasawara, M. F. Toney, A. Nilsson, *Nat. Chem.* **2010**, *2*, 454–460.
[25] M. Oezaslan, F. Hasché, P. Strasser, *J. Electrochem. Soc.* **2012**, *159*, B444.

Manuscript received: January 10, 2020
Accepted manuscript online: January 16, 2020
Version of record online: February 18, 2020

